I Turner et al.

An RF Ion Source Model for H- Production Without Caesium

An RF ion source model for H⁻ production without caesium

I Turner[1], A J T Holmes[2], J Zacks[1] and R McAdams[1]

[1] United Kingdom Atomic Energy Authority, Culham Centre for Fusion Energy, Culham Science Centre, Abingdon, Oxon, OX14 3DB, UK.
[2] Marcham Scientific, Hungerford, Berkshire, RG17 0LH, UK.

E-mail: Ingrid.Turner@ukaea.uk

Abstract

A 1D model of an RF driven ion source based on ionisation by thermal electrons is presented. The RF source differs from traditional filament and arc ion sources because there are no primary electrons present, and is simply composed of an antenna region (driver) and a main plasma discharge region. However the model does still make use of the classical plasma transport equations for particle energy and flow, as used previously in DC source models where they have worked well. The model currently uses the geometry and other source parameters of the Small Negative Ion Facility (SNIF) ion source at CCFE and only considers the hydrogen ion species, but may be easily adapted to model other RF sources. The model provides a detailed description of the plasma parameters along the source axis, i.e. plasma temperature, density and potential, as well as current densities and species fluxes, but does not consider the RF matching unit. The inputs to the model are the source geometry, RF power, the magnetic filter field, the source gas pressure and the plasma grid insert bias. Results from the model are presented and where possible compared to existing experimental data from SNIF, with varying RF power, source pressure and insert bias.

Keywords: RF ion source, negative ions, SNIF

Symbols used in the paper

A table is provided below of all the parameters shown in this paper that are not defined explicitly by equations, with the exception of any rate coefficients, which are listed separately in the text.

Table 1 Definitions of symbols used in the paper

Symbol	Description
A_a	Plasma window area
A_G	Plasma grid area
β	Average ion loss along the source
B_c	Cusp field
B_x	Magnetic field transverse to source axis
C_1, C_2, C_3	Flux fractions of positive hydrogen ions
C_{tot}	Total sidewall cusp length
δ	Effective plasma depth
d_i	Insert depth
E_y	Radial component of electric field - extraction section
f_e	Electron grid current fraction
f_i	Ionic grid current fraction
F_T	Sum of ion fluxes at each step in the transport equations
k	Coulomb coefficient
λ_C	Coulomb logarithm
L_d	Distance from backplate to beginning of filter field
L_m	Filter field characteristic distance
M	Flux weighted ion mass
n_a n_G	Plasma density at antenna and grid
N_{gas}	Gas density
N_H	Atomic hydrogen density
N_{H2}	Molecular hydrogen density
ν_e	Electron collision frequency
ω, Ω	Larmor frequency for electrons and ions respectively
P_{gas}	Power removed by cooling at the source walls
ϕ_a ϕ_G	Plasma potential at antenna and grid
P_{rf}	RF input power
q	Fractional negative ion density
S_D	Source depth
Q_{e+H^-}	Energy flux of negative plasma particles
ρ_e ρ_i	Larmor radii for electrons and ions
T_a T_G	Electron temperature at antenna and grid
t_H	Wall loss time for vibrational molecules
U_{e+H^-} U_i	Particle flux of negative plasma particles, and positive ions respectively
V_G	Plasma grid potential
V_{insert}	Bias insert potential

1. Introduction

Modelling a radio frequency discharge normally starts with the antenna circuit and examines the plasma as a component in that circuit via the plasma impedence. The model of Gudmundsson and Lieberman [1] uses this approach. This paper takes the opposite approach and begins instead with the ionization process via the hot plasma electrons in a hydrogen discharge. The source has internal magnetic fields created by bar magnets to form a magnetic filter as in DC sources, with the aim of enhancing both H⁻ negative ion formation [2,3,4] and also the proton fraction [5,6,7]. Electric fields are also present, generated by the RF system and plasma discharge. This approach lends itself to the use of the transport coefficients described in the paper by Surrey and Holmes [6,7].

The same methodology can be used, originally developed by Epperlein and Haines [8], to create a 1-D model of the discharge plasma [6,7], except that now (unlike the DC arc sources) there are no fast primary electrons and all the ionization is made by the hot tail of the plasma electron energy distribution. This causes a significant change to the modelling approach which is described in this paper. The model can be applied to both the extraction of the species of positive ions (H⁺, H₂⁺, H₃⁺) or alternatively to the extraction of negative ions (H⁻) without the use of caesium. In the latter case it also deals with the co-extraction of electrons. For this report, the model is applied to the Small Negative Ion Facility ion source [9] which is described in Section 2. The model itself is described in Section 3 and the results discussed in Section 4.

2. The SNIF ion source

The SNIF ion source is shown in figure 1(a). The SNIF ion source is a cylindrical source, 280mm in diameter and 220mm deep internally. The source walls are copper with stainless steel flanges for holding the grids, an aluminium feedthrough flange at the extraction plane, and a 150mm diameter, 10mm thick quartz window on the backplate, through which the flat spiral RF antenna can couple to the plasma. The source is driven by a 5kW RF generator operating at 13.56MHz, with an auto-tuning "L" matching network.

Magnets are located on the outside of the source body in a checkerboard arrangement, with a dipole filter field set up near the extraction plane. This dipole field allows a region of lower temperature plasma to be created where a greater density of negative ions can be produced. There is also a magnetic field present from the accelerator magnets which strays into the source. The total magnetic field along the source axis is shown in figure 1(b).

The plasma grid contains a 63mm diameter biased insert plate, containing the 14mm diameter extraction aperture (area = 154mm²). During extraction, this grid will normally have a positive bias with respect to the anode, allowing a suppression of the electrons co-extracted within the beam.
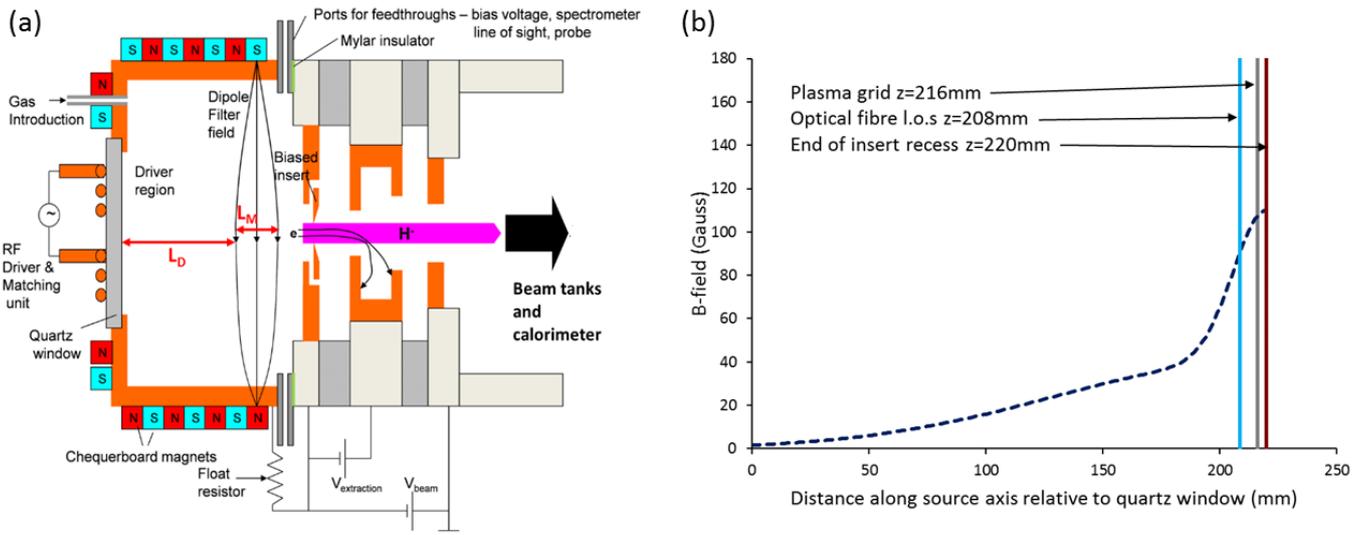
FIGURE 1. (a) Schematic of the SNIF Ion source and accelerator. (b) Magnetic field from filter and accelerator magnets along the central beam axis in the source from the antenna window up to the end of the biased insert recess.

The feedthrough flange, 10mm thick, is located between the main source body and the plasma grid. As well as being used as a feedthrough for the bias supply connection, this flange is used for diagnostics, including an optical fibre to a McPherson 209 spectrometer (focal length = 1.33m) with an Andor Newton CCD detector, allowing measurements of the Balmer and Fulcher spectra along a line of site parallel to, and approximately 8mm from, the plasma grid, with resolution up to 0.007nm.

The SNIF accelerator is a triode design, capable of producing an H⁻ beam of energy 30kV, with the plasma grid held at -30kV, and the beamline at earth potential. There is a small resistance (20Ω) between the plasma grid and the source, allowing the source to float with the plasma potential. The grids are copper, with a single beam aperture, and contain a series of neodymium iron boron (NdFeB) magnets to deflect co-extracted electrons on to Grid 2, whilst minimizing deflection of the H⁻ ions. The extraction grid (Grid 2) is operated at between 2-4 kV above the plasma grid, depending on the beam perveance required.

The beamline consists of two joined 1000 litre tanks containing two visible cameras: one mounted on the side, the other on the top. The image quality from the cameras is not particularly high, however they do allow for visual beam monitoring so that the effects of changing the beam perveance can be easily observed.

The original SNIF beam target was a castellated copper calorimeter, instrumented with over 100 thermocouples and creating a grid with 5mm by 5mm resolution. Modelling of this calorimeter using ANSYS has allowed the power loading on the calorimeter to be calculated, giving an indirect measurement of the beam current.

Due to the low beam current on SNIF, and the physical contact of the calorimeter to the steel vacuum tanks, pulses of a notable length (~15s) were required in order to obtain a temperature rise of just a few Kelvin, making the reliability of measurements harder. As such, this target has now been replaced with a Faraday cup, which, when fully commissioned, is expected to provide a more direct and reliable measurement of beam current.

3. The basic concept

All the ionization that takes place throughout the source volume is set by the local ionization rate which is determined by the local electron temperature and density together with the gas density, N_{gas}. The ionization diminishes as we move towards the magnetic filter as the plasma cools and this filter field, which peaks at a distance L_d from the antenna window, has a presumed Gaussian profile with a characteristic distance, L_m. Finally at the other end of the source there is an extraction plane at a distance, S_D, from the antenna wall. The power absorbed by the plasma, P_{rf}, is the defining parameter together with the source geometry and the gas pressure. This power can be related to the total ionization current, I_{ion}, the incident power and the reflected power in the antenna circuit. However the antenna circuit modelling is not presented here.

The external bar magnets create magnetic confinement on the side walls with an effective hybrid Larmor radius, ρ (which is defined as $= \sqrt{\rho_e \rho_i}$), on a total cusp length, C_{tot}, so that the sidewalls have a plasma loss area, A_{wallc} given by $A_{wallc} = 4C_{tot}\rho$. Note that cusp lines on the back of the source are considered as part of the side wall. This is discussed further in

section 3.2. The factor of 4 is in common with other source models [6,7] and was first proposed by Leung, Hershowitz and Mackenzie [10].

3.1 The Antenna Region

Gudmundsson and Leiberman [1] introduced an energy balance equation: each ionisation process leads to a loss of energy for the plasma which is described by ε in equation (1):

$$\varepsilon = \varepsilon_H + \varepsilon_e + \varepsilon_i \tag{1}$$

where ε_e and ε_i are the energies removed by electrons and ions respectively as they escape from the plasma. The expressions for the ionization energy, ε_H, are derived from Hjartarsen et al [11] and are expressed as empirical formulae so that they can be used in an iterative convergence procedure. In our model, the energy to create a single electron-ion from molecular hydrogen is expressed as:

$$\varepsilon_{H2} = 22\exp\left(\frac{8.5}{T_a^{0.5}}\right) \tag{2}$$

The analogous expression for atomic hydrogen is:

$$\varepsilon_H = 26\exp\left(\frac{2}{T_a^{0.7}}\right) + 20000\exp(-3T_a^2) \tag{3}$$

In equations (2) and (3) above the units of energy and temperature are expressed in units of eV. These two empirical fitting curves agree closely with the Hjartarsen data over 1 – 100eV electron energy range.

The energy of the escaping electrons to the source wall is $\varepsilon_e = 2T_a$ and that of the ions is $\varepsilon_i = \phi_a + T_a/2$ where ϕ_a is the plasma sheath potential in the region between the antenna and magnetic filter [12]. This is the floating potential of the plasma relative to the quartz window and sidewalls but not the plasma grid which floats at a different potential, ϕ_G. There may be an additional potential on the plasma grid if we apply a bias potential, V_G, between sidewalls and grid. For convenience, the plasma potential ϕ itself is defined as zero and all other surfaces are negative, so the quartz and sidewalls are at -ϕ_a volts relative to the plasma. Thus ϕ_a and ϕ_G (plasma potential at the grid) are positive numbers.

This ion energy loss includes the ion energy gained in crossing the sheath (slightly bigger than in [1] as it includes the pre-sheath voltage). The fractional atomic gas density, F, is defined as:

$$F = \frac{N_H}{N_H + N_{H2}} \tag{4}$$

where N_H and N_{H2} are the densities of hydrogen atoms and molecules respectively.

We can introduce a power balance equation using the rf power, P_{rf}, supplemented by the bias power, $I_G V_G$, and equating it to the power removed by escaping ions and electrons and power removed by gas cooling on the walls, P_{gas}:

$$I_G V_G + P_{rf} = [F(\varepsilon_H + 2.5T_a + \phi_a) + (1 - F)(\varepsilon_{H2} + 2.5T_a + \phi_a)]\alpha I_{ion} + P_{gas} \tag{5}$$

The above equation requires knowledge of the likely temperature variations along the source axis. However this is not derived until much later in the code, therefore to get around this problem, the parameter α is introduced as an empirical averaging constant, given that ε_H, ε_e and ε_i are calculated based on values at the antenna end of the source. α represents the actual values of the ionisation energies (ε_H and ε_{H2}) integrated over the length of the source and weighted by the local plasma density, as opposed to using just the values obtained at the antenna. As ε_H and ε_{H2} rise as the electron temperature falls, it is expected that α is greater than unity. A value of 1.4 is used in this model as it is close to what occurs.

The term I_{ion} is the **total** current of ions or electrons (which are of course equal). Note that any potential across the filter region does not alter the above equation as all the ions and electrons are assumed to be born near the antenna where the electron temperature is T_a and the plasma sheath voltage is ϕ_a. The net current to the quartz plate is zero by definition but there could be a current, I_G, flowing to the plasma grid with an equal but opposite current flowing to the sidewalls. This current is assumed to be positive and ionic (so a negative value would correspond to an electron flow to the grid). Real power is associated with this grid current, so it is added to the absorbed RF power, P_{rf}. This is discussed later in the paper.

Given the equal currents of ions and electrons to the antenna window, I_a, we can write:

$$\frac{I_a}{A_a} = 0.55 \times 0.73 \times en_a \left(\frac{eT_a}{M}\right)^{0.5}$$
$$= \frac{0.73 en_a v_e}{4} \exp\left(-\frac{\phi_a}{T_a}\right) \tag{6}$$

where M is the ion mass which is the flux weighted average over the three hydrogen ion species (H$^+$, H$_2^+$, and H$_3^+$), A_a is the plasma window area, n_a is the plasma density at the antenna and v_e is the electron velocity. The factor of 0.55 arises from a Tonks-Langmuir sheath where ionization takes place right up to the sheath edge. The normal sheath (as in DC sources where ionization occurs elsewhere) has a factor of exp(-0.5) = 0.61 instead. Equation 6 also contains a multiplication parameter of 0.73. This was introduced in reference [1] to account for the reduction in plasma density at the antenna surface at the back of the source. After eliminating variables on the RHS and LHS of equation 6, it can be reduced to the following:

$$\exp\left(-\frac{\phi_a}{T_a}\right) = 1.379\left(\frac{m_e}{M}\right)^{0.5} \tag{7}$$

Thus if we know T_a, and have a knowledge of M, ϕ_a is found and hence equation 5 fixes the total ionization current I_{ion} once P_{gas} and $I_G V_G$ are determined.

3.2 The main discharge

A shape coefficient is needed to describe the plasma production over the source dimensions. This is accomplished differently to [1]. We make the basic assumption that the plasma is completely uniform in the radial direction as we do not expect there to be significant lateral loss of plasma (although the concept of radial cusp losses is retained as seen below). The total ionic current, I_{ion}, flows to three surfaces; the quartz plate, I_a, the sidewalls, I_w, and the grid, $f_i \times I_{ion}$. There is also a recombination current, I_{rec} via the dissociative recombination reaction between H_3^+ and electrons. Summing the currents gives:

$$I_{ion} = I_a + I_w + f_i I_{ion} + I_{rec} \tag{8}$$

The factor f_i represents the fraction of the total ionization current, I_{ion}, going to the plasma grid. For convenience, we assume that the temperature of those electrons going to the plasma grid is T_G. Using the derivation of the hybrid Larmor radius as in the DC model [6,7] the sidewall loss area (defined earlier), A_{wallc} is:

$$A_{wallc} = 4\rho C_{tot}$$
$$= \frac{4C_{tot}}{eB_c}[M\psi_i(0.5+\eta)^{0.5}m_e\psi_e]^{\frac{1}{2}}\beta T_a^{\frac{1}{2}} \tag{9}$$

where

$$\psi_i = \left(\frac{e}{M}\right)^{\frac{1}{2}} \quad \psi_e = \left(\frac{8e}{\pi m_e}\right)^{\frac{1}{2}} \text{ and } \quad \eta = \frac{\Phi_a}{T_a}$$

and β is defined by

$$\beta = \frac{\int_0^{S_D} nT\psi_z \, dl}{S_D n_a T_a \psi_c}$$

and represents the average loss along the length of the source. S_D is the source depth. The electron velocity term ψ_e is later replaced by a composite term ψ_c which contains the negative ion velocity term ψ_{neg} and mixes the two using the negative ion fraction q as seen in section 3.5. the term ψ_z is another composite term equivalent to ψ_c but in the filter region and B_c is the surface cusp field. Returning to equation 8 it becomes

$$I_{ion} - I_{rec} =$$
$$en_a\left(\frac{eT_a}{M}\right)^{\frac{1}{2}}(0.4A_a + 0.61A_{wallc}) + f_i I_{ion} \tag{10}$$

The reason why the nT product is averaged and not $nT^{0.5}$ arises from the fact that the hybrid Larmor radius also depends on the temperature. As the cusp losses are expected to be roughly proportional to the local plasma density, a simple average value of $\beta = 0.5$ is used ***initially***. Later a better averaging technique is developed as seen in section 3.4.

The total ion current, I_{ion}, must be equal to the total ionization so:

$$I_{ion} = en_a\delta S_D A_G\big(N_H S_1(T_a) + N_{H2} S_2(T_a)\big) \tag{11}$$

where A_G is the plasma grid area and δ is the effective depth of the plasma where the ionization rates for atomic and molecular hydrogen, S_1 and S_2 respectively, remain at the level set in the driver region at a temperature and density T_a, n_a. Thus:

$$\delta = \frac{\int_0^{S_D} n\big(N_H S_1(T) + N_{H2} S_2(T)\big) \times dl}{S_D n_a\big(N_H S_1(T_a) + N_{H2} S_2(T_a)\big)} \tag{12}$$

Initially we can set δ to say 0.5 and then update it together with β once the plasma profile has been found, as well as new values of the atomic and molecular gas densities, N_H and N_{H2}. The values of β and δ are updated after each main cycle of calculation and the iteration is continued until a satisfactory convergence is achieved.

The methods used for dealing with the atomic gas fraction, atomic temperature and the gas accommodation coefficients is identical to that used in the model for the DC sources [6,7] and will not be repeated here in the interests of brevity. The reaction rates used for the ionisation processes and the production of atomic hydrogen are also identical to those used in the DC source and are denoted by the following labels in this paper:

- Ionisation of atomic hydrogen – S_1
- Ionisation of molecular hydrogen – S_2
- Dissociation of molecular hydrogen – S_3
- H_2^+ recombination – S_4
- H_2^+ dissociation to protons – S_5
- Formation of H_3^+ ions – S_6
- H_3^+ dissociation – S_7
- H_3^+ recombination – S_8

3.3 The plasma drift and filter region

Unlike in reference [1], in our model the plasma flow is controlled by the Epperlein and Haines equations [8] in a manner very similar to that used in the magnetic filter sources described by Surrey and Holmes [6,7]. These equations are:

$$U_{e+H^-} = \frac{I_{ze}\,F_T}{e(I_{ion} - I_{rec})}$$

$$= \frac{-enE - eT_e\frac{dn}{dz}}{m_e \nu_{e1}\left(1 + \left(\frac{\omega}{\nu_{e1}}\right)^2\right)} + \frac{en\frac{dT_e}{dz}}{2m_e \nu_{e2}\left(1 + \left(\frac{\omega}{\nu_{e2}}\right)^2\right)} \qquad (13)$$

$$Q_{e+H^-} = U_{e+H^-}\,\Phi_a$$

$$= \frac{-enT_eE - eT_e^{\,2}\frac{dn}{dz}}{m_e \nu_{e1}\left(1 + \left(\frac{\omega}{\nu_{e1}}\right)^2\right)} + \frac{1.92enT_e\frac{dT_e}{dz}}{m_e \nu_{e2}\left(1 + \left(\frac{\omega}{\nu_{e2}}\right)^2\right)} \qquad (14)$$

$$U_i = \frac{I_{zi}\,F_T}{e(I_{ion} - I_{rec})} = \frac{enE - eT_i\frac{dn}{dz}}{M\nu_i\left(1 + \left(\frac{\Omega}{\nu_i}\right)^2\right)} \qquad (15)$$

where the collision frequencies are defined as:

$$\nu_{e1} = N_{gas}S_{el} + 2\lambda_c nkT^{-3/2}$$

$$\nu_{e2} = 2\lambda_c nkT^{-3/2} - 2N_{gas}S_{el}$$

$$\nu_{i1} = N_{gas}S_6\sqrt{2} + \frac{1.4\mathrm{x}10^{-12}}{T^{-3/2}}$$

$$\nu_{i2} = N_{gas}S_6 + \frac{1.4\mathrm{x}10^{-12}}{T^{-3/2}}$$

$$\nu_{i3} = N_{gas}S_6\sqrt{2/3} + \frac{1.4\mathrm{x}10^{-12}}{T^{-3/2}}$$

as in reference [6]. Please refer to table 1 for definitions of the other symbols used in the above equations. Negative ions are treated as "heavy" electrons as the negative charge oscillates between being an electron or a negative ion. This method of dealing with negative ions within the plasma is identical to that used in references [6] and [7] and is described in greater detail below. S_{el} is the rate for elastic collisions between gas molecules and electrons and has a value $S_{el} = 3\mathrm{x}10^{-14}(1-\exp(-T))\mathrm{m}^3\mathrm{s}^{-1}$, and k is the Coulomb coefficient with a value of $7.7\mathrm{x}10^{-12}\mathrm{m}^3\mathrm{eV}^{1.5}\mathrm{s}^{-1}$. The terms I_{ze} and $I_{zi,}$ which are the electron and ion currents respectively going to the grid, are defined by:

$$I_{ze} = f_i f_e I_{ion} \quad \text{and} \quad I_{zi} = f_i I_{ion}$$

The equations 13 and 14 apply to the negative charge carriers (electrons and negative ions) and equation 15 applies to the positive ions. There is no energy flux equation for the positive ions as these ions are very closely coupled to the gas by frequent collisions and the positive ion temperature is made equal to the gas temperature. As the negative charge carriers oscillate between being electrons and H⁻ ions, only a single transport equation for flux and energy flow is used with a weighting term, q, being used to assign the value of the collision frequency and cyclotron frequency between the electron value and H⁻ value. This allows a single plasma density, *n*, to be used with the term *q*, determining the fractional density of negative ions relative to the positive ions (whose combined density is equal to the plasma density). The temperature of the negative ions is assumed to equal to that of the electrons as to do otherwise would cause considerable mathematical difficulty. The exact value of q is described in detail in section 3.5.

Testing of the transport equations shows that while the plasma density decreases fairly rapidly from the start line of the calculation, the temperature declines slowly with distance. The plasma potential variation is intermediate between the two and exhibits a significant change from the driver region to the extraction region. These conclusions are similar to those in [1].

There are several boundary conditions at the plasma grid. The grid current, I_G can be written as:

$$I_G = I_{ion}f_i(1 - f_e) \qquad (16)$$

Thus a positive value of I_G corresponds to ion collection (to match the potential, V_G). Firstly the ion current fraction, f_i, should be evaluated and updated from the grid plasma density and temperature:

$$f_i = \frac{0.61n_GeA_G\left(\frac{eT_G}{M}\right)^{1/2}}{I_{ion}} \qquad (17)$$

The parameters subscripted with "G" are the values calculated at the plasma grid e.g. n_G is the plasma density at the grid.

To avoid violent changes in f_i (must be <1%), this equation could not be used in the RF source, therefore f_i is incremented by a small fixed amount e.g. 0.0001, so that the convergence point is not missed. Thus values are created for I_{ion}, n_G, T_G, ϕ_G and f_i (the revised value). A choice must then be made: define V_G and create a value for f_e and hence I_G or, alternatively, define f_e as a fixed value at the start and find V_G. The latter method has been chosen because V_G has no direct influence on the transport equations. At the end of the transport loop, the ion current to the grid can be found, and since f_e is used as input, the grid bias voltage can also be found from the electron grid current as follows:

$$I_{Gi} = 0.61A_G n_G e\psi_i T_G^{1/2} \qquad (18)$$

$$V_G = ln\left(\frac{4I_{ge}}{\psi_z n_G A_G e \sqrt{T_G}}\right) T_G + \phi_G \qquad (19)$$

where $I_{Ge} = I_{ion} f_i f_e$ (electron grid current) with the new value of f_i.

The grid bias, V_G, is positive if the grid is biased negatively to the sidewalls and equation 19 assumes that normally all potentials have a positive numerical value. Finally a new grid current, I_G, can be found from equation 16.

3.4 Deriving the averaging coefficients δ and β

The value of the local plasma density, n and temperature, T as a function of position along the source axis has now been found from the solution of equations 13 to 15, based on the previous values of all these constants (initially β and δ are 0.5). Averages of plasma density and temperature (n and T) over the current and previous steps (i and i-1) are then taken (so that we have $\bar{n}$ and $\bar{T}$) and used to update the constants. In the case of δ, the updated value is:

$$\delta = \frac{\int_0^{S_D} \bar{n}\left(N_H S_1(\bar{T}) + N_{H2} S_2(\bar{T})\right) dl}{S_D n_a \left(N_H S_1(T_a) + N_{H2} S_2(T_a)\right)}$$

This is derived by calculating the value at step *i* of:

$$Sum_1 = N_H dl \sum_i \bar{n} S_1(\bar{T}) \text{ and } Sum_2 = N_{H2} dl \sum_i \bar{n} S_2(\bar{T})$$

These are added for all steps from the start line to the grid at *l* = S_D. The new values of N_H and N_{H2} derived as described in references [6,7] in both the numerator and denominator are used and in the next cycle this updated value of δ is used.
The term β is similarly found:

$$\beta = \frac{\int_0^{S_D} \bar{n}\bar{T}\psi_z dl}{S_D n_a T_a \psi_c}$$

The potential, ϕ, is the local plasma potential derived from the transport equations (E = -dϕ/dz). As with n and T, ϕ is averaged over the current and previous steps, so that we have:

$$\bar{n} = \frac{(n[i-1] + n[i])}{2}$$

$$\bar{T} = \frac{(T[i-1] + T[i])}{2}$$

$$\bar{\phi} = \frac{(\phi[i-1] + \phi[i])}{2}$$

3.5 The negative ions

The negative ions are formed by dissociative attachment collisions between vibrationally excited hydrogen molecules and cold electrons whose temperature is less than 2eV [13]. This is expressed by a single rate coefficient S_{DA}, which is a function of electron temperature for collisions between molecules whose vibrational level is greater than 8. Vibrational levels below 8 have a rate which is essentially zero in comparison. Above an electron temperature of 2eV, the rate coefficient decreases rapidly and at the same time the electron detachment rate rises significantly, sharply reducing negative ion formation.

The vibrationally excited molecules are formed by collisions between the high energy electrons in the "hot" tail of the electron distribution and molecules in the lowest vibrational state (υ = 0). Some of these are then destroyed by inelastic (ionising or excitation) collisions with electrons and additionally by collisions with atomic hydrogen [13]. The vibrational molecules also cannot survive more than a few interactions with the source walls, which is accounted for by introducing a survival time t_H, also known as the wall loss time. A rate equation for the vibrational density can thus be formed:

$$N_{(v \geq 8)} n_a \frac{R_{in}}{T_a} + \frac{N_{(v \geq 8)}}{t_H} = N_{H2} n_a S_p \qquad (20)$$

The vibrational density $N_{(v \geq 8)}$ is assumed to be uniform throughout the plasma chamber as it was in the DC model [6]. The term S_P is the rate coefficient for production from vibrational levels with $v \geq 8$ and has a value of 7.5×10^{-15} m³/s [14]. The value of t_H depends on three factors: the gas temperature, the size of the source and lastly the number of wall collisions before de-excitation. Karo and Hiskes [15] have argued that the collision number should be approximately 4. The destruction rate is the same as the total inelastic collision rate, R_{in}, developed by Hiskes and Karo [14] and used in the equivalent section of the DC code [6,7].

A similar rate balance equation can be written for the negative ions (Holmes [16]). The production rate, S_{DA}, by dissociative attachment with vibrationally excited molecules above $v = 8$ is balanced by losses by ion-ion recombination with a rate, S_{II}, electron detachment with a rate, S_{EV}, and also loss by atomic gas collisions with a rate, S_H. The rate for electron detachment, S_{EV}, and the dissociative attachment rate, S_{DA}, depend strongly on the local electron temperature as described in [6]. The SNIF source only operates with a low plasma density unlike that in reference [6], therefore the mean free path for negative ions is a significant fraction of the source dimensions. However there are no wall losses of negative ions because the source operates with a positive plasma potential (see section 4, figure 5), so providing strong negative ion confinement. This gives a second balance equation:

$$N_{(v \geq 8)} n_e S_{DA} = n_- n_e S_{EV} + n_- N_H S_H + n_- n_+ S_{II} \quad (21)$$

Replacing the negative ion density, n_-, by the fractional negative ion density, $q = n_-/n_+$, (hence n_e becomes $n_+(1-q)$) and assuming local plasma neutrality, gives a quadratic equation in q:

$$0 = -n_a S_{EV} q^2 + q\left(n_a(S_{EV} + S_{II}) + N_H S_H + N_{(v \geq 8)} S_{DA}\right) - N_{(v \geq 8)} S_{DA} \quad (22)$$

where $n_a = n_+$ (positive ion density) at the antenna. This expression is also used in [6].

If the local value of the plasma electron temperature, T and plasma density n, as well as the value of the vibrational density from (21) are all known, the value of q can be found, so deriving the electron and negative ion densities. Solving the above quadratic shows that the fractional density, q, of negative ions depends on the various cross-sections but is never zero and we can assign an effective weighted mass dependent on the value of q as well as an effective collision frequency.

The terms in the equations 13 and 14 have to be weighted for the presence of negative ions which allow the electrons to move through the magnetic fields far more easily than would be expected. As all electrons spend part of their existence as a negative ion, the term, q, can be used as a weighting term for this effect, and the hybrid collision frequencies (weighted versions of ν_{e1} and ν_{e2} from section 3.3) are defined:

$$\nu_{e1} = (1-q)\left(N_{gas} S_{el} + 2\lambda_c nkT^{-3/2}\right) + q\left(N_{gas} S_{neg} + 2nk_{neg} T^{-3/2}\right)$$

$$\nu_{e2} = (1-q)\left(2\lambda_c nkT^{-3/2} - 2N_{gas} S_{el}\right) + q\left(2nk_{neg} T^{-3/2} - 2N_{gas} S_{neg}\right)$$

where $S_{neg}=1.6 \times 10^{-16} m^3 s^{-1}$ and $k_{neg}=7.0 \times 10^{-13} m^3 eV^{1.5} s^{-1}$. S_{neg} and k_{neg} are the equivalent of S_{el} and k for negative ions. These hybrid collision frequencies also enter into the cyclotron element of the transport equations in the filter field region.

3.6 The positive ion species

The directed initial current density of ions and electrons towards the plasma grid is zero at the plane of origin at the back of the source, as no ionization has yet taken place. By analogy, the directed electron energy flux is also zero. The ionic grid current is defined as a fraction, f_i, of the total ion production and the electron current is a further fraction, f_e of this current. The latter has an initial value close to unity while the former is close to zero.

In the equations below, the velocities in the denominator are the mass weighted thermal ion velocities based on the gas temperature which is also the effective ion temperature due to the high ion-neutral collisionality. After each step the total fluxes of all ion species are re-evaluated by integrating the following expressions from the source antenna plasma to the plasma grid, exactly as in reference [6].

$$F_1[i] = F_1 + \left[nS_1(T)N_H e + \frac{F_2 n S_5}{v_{i2}} + \frac{F_3 n S_7}{v_{i3}}\right] dl$$

$$F_2[i] = F_2 + \left[nS_2(T)N_{H2} e - \frac{F_2 n S_5}{v_{i2}} - N_{H2} F_2 \sigma_6\right] dl$$

$$F_3[i] = F_3 + \left[N_{H2} F_2 S_6 - \frac{F_3 n S_7}{v_{i3}} - \frac{F_3 n S_8}{v_{i3}}\right] dl$$

After integration from the backplate to the plasma grid, the total directed ion flux, F_{ig}, is composed of the three individual fluxes, F_{1g}, F_{2g} and F_{3g}:

$$F_{ig} = \left(F_{1g} + F_{2g} + F_{3g}\right) \quad (23)$$

with fractions:

$$C_1 = \frac{F_{1g}}{F_{ig}} \quad C_2 = \frac{F_{2g}}{F_{ig}} \quad \text{and} \quad C_3 = \frac{F_{3g}}{F_{ig}}$$

The three C values above affect the ion transport coefficient $M\nu_i\left(1 + \left(\frac{\Omega}{\nu_i}\right)^2\right)$ in equation 15. This is included by averaging over the three ion species using the appropriate ion mass and altering ν_i and Ω as required. The three resulting values are then weighted by the ion flux fractions to create a mean value to be used in equation 15. Note that if the electrons spend part of their time as negative ions, the electron density in the collision frequency, ν_i, is reduced by this factor. These expressions assume that the ions all have the same temperature. The value of the average mass number of the ion species mix, A_{mass}, is then:

$$A_{mass} = \left(C_1 + \frac{C_2}{\sqrt{2}} + \frac{C_3}{\sqrt{3}}\right)^{-2} \quad M = A_{mass} m_p$$

as it is based on fluxes not densities. Thus the ion mass M is also updated as above. Note that the above expressions refer to hydrogen discharges only.

The fraction of the total ion current that goes to the plasma grid is only part of the total ion production, typically ~60%, with the rest going to the anode or the quartz plate. The addition of a magnetic filter increases the latter currents significantly and reduces the former current. These new fractions are used in the entire transport calculations (13 to 15) to define the average ionic transport coefficient for the cycle that follows the definition of the C_1, C_2 and C_3 values.

The electron current to the plasma grid is a low fraction of the total electron production in almost all situations. The values of f_e and f_i are found by iteration over many cycles so that they match the assumptions about the plasma grid current, I_G, which forms part of the input data. However it is necessary to guess the values initially but these are updated in later cycles.

If all the three ion flux gradients are added, all of the cross terms cancel apart from the S_8 term. This last term is the recombination of H_3^+ and n_e and represents a loss of ionization. Thus:

$$I_{rec} = A_g \int_0^{S_D} \frac{\langle F_3 n \rangle S_8}{v_{i3}} dl \qquad (24)$$

This current is included in the total ion current balance but is usually quite small and can be simply summed at each step.

3.7 Solving the plasma equations

The following flow chart gives a summary of how the main processes in the code and how it solves the equations. The extraction part of the model is described in section 3.8. The current version of the model is written in Interactive Data Language (IDL) and runs in a UNIX environment. The model is primarily set up for the SNIF source geometry and filter field but these can easily be modified for other sources. The user inputs into the code are the RF absorbed power, the source filling pressure and the insert bias potential. Typically the code takes ~20 minutes to run and achieves convergence within approximately 10,000 major cycles.
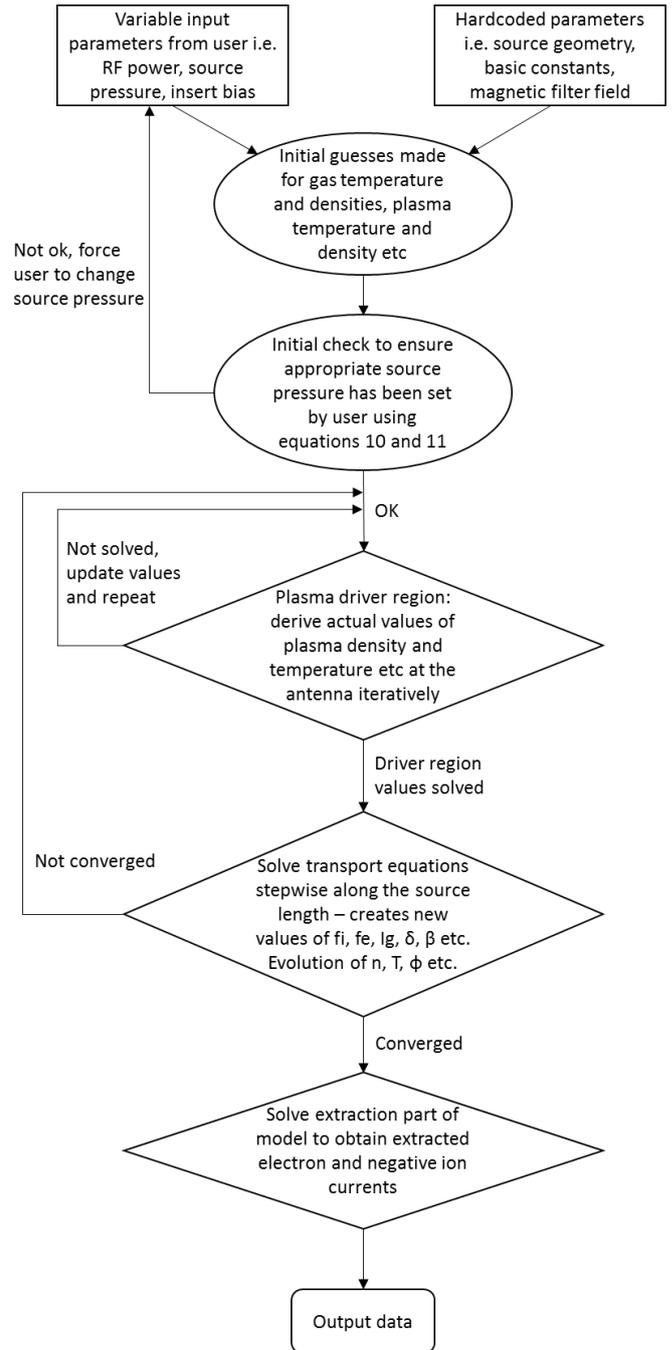
FIGURE 2. Flow chart showing operation and data flow in the main code

3.8 Electron extraction

Once the electrons and negative ions enter the recess where the extraction aperture is situated, negative ion production ceases and extraction begins. This process was originally examined by Haas and Holmes [17] and uses the Boltzmann

equation as its basis and then derives a model for the electron current extracted through the extraction orifice.

Using the transverse axis, y, which is orthogonal to the magnetic field in the x direction and source axis (z), the electron flow in the y direction can be written:

$$n_e m_e \nu_e \mathrm{v}_{ey} = -eT_e \frac{dn_e}{dy} - en_e(E_y + \mathrm{v}_{ez}B_x)$$

Across the insert, it is assumed that dn/dy is zero (a uniform plasma) and there is no electric field in the y direction (consistent with the general assumption that over short scales the plasma is homogenous in x or y). Thus:

$$en_e \mathrm{v}_{ez} B_x = -n_e m_e \nu_e \mathrm{v}_{ey} \qquad (25)$$

This is also equation 8 in [17].

Consider a circular insert of recess radius, R, and depth d_i. The incoming total electron flux, I at z, flowing in the axial (z) direction is:

$$I = en_e(z)\mathrm{v}_{ez}(z)\pi R^2$$

where n(z) is now the local density at the point considered (z) inside the insert recess. The lateral loss, *ΔI*, over a short segment, *Δz,* of the depth at this position is (note only a semicircular loss area is considered as the electrons only go in one direction)

$$\Delta I/\Delta z = -2eRn_e(z)\mathrm{v}_{ey}\,G(\Phi) \qquad (26)$$

where G is the function that determines the sheath effect. The term Φ is given by the insert to plasma potential which is:

$$\Phi = -(\phi_g - V_g) + V_{insert}$$

where V_{insert} is the potential of the biased insert in the SNIF accelerator (see figure 1). The potential Φ can be positive or negative depending on the value of V_{insert}, therefore G has two forms, one where there is a standard sheath retarding potential and the other if the electrons are accelerated into the insert:

$$G(\Phi) = \exp(\Phi/T_G) \qquad\qquad \Phi < 0$$

$$G(\Phi) = (1 + 2\Phi/T_G)^{0.5} \qquad \Phi > 0$$

The positive Φ equation is identical to ion accelerating sheaths in plane probe theory. The multiple of 2 in this equation has previously been shown by McAdams et al [18] equation 22.

Eliminating the transverse velocity, v_{ey} between equations 25 and 26 yields:

$$\frac{dI}{dz} = -\frac{2eB_x G(\Phi)}{\pi Rm v_e}\,I$$

Integrating and dividing by πR^2 gives the axial electron current density, J:

$$J = J_0 \exp\left[-\frac{2eG(\Phi)\int_0^{d_i} B\,dz}{\pi Rm v_e}\right] \qquad (27)$$

This is almost identical to equation 22 in [17] for negative values of Φ and comparison of actual values gives an almost identical argument. The term, J_0, is the electron current density from the plasma at the entrance to the insert and is the same as the electron flux to the entire surface of the plasma grid.

However there are some considerable differences in behaviour compared with the Haas-Holmes model [17]. The scaling with B is obviously the same as is the Φ dependence inside the exponent. However in [17] the exponent only depended on $T_e^{-0.5}$ through the electron velocity. Now this is replaced by the $1/Rmv_e$ term which argues that the loss is inversely proportional to the insert radius, R. Thus the attenuation gets much more severe if the insert has a small diameter as expected from equation 27. As the electron and negative ions enter the insert recess, their density drops rapidly because their velocities become large due to acceleration. A very approximate estimate therefore is to use half the initial value of density in the calculation of attenuation.

The entire source chamber could be considered as a very large insert, but the large radius of 130mm makes the exponent close to zero, providing the source filter field is not too large. There is also wall cusp shielding giving a further reduction in electron loss by the ratio of 4ρ/H where ρ is the hybrid Larmor radius of the plasma cusps on the source body and H is the inter-cusp distance. In contrast, the insert region has a very rapid attenuation due to its small size and high field.

Thus in the main code all that is needed is to reduce the electron flux by the factor in equation 27 above, starting at the beginning of the insert until the knife-edge of the actual extraction aperture is reached at the depth, d_i. A similar attenuation equation is applied to the negative ion current density, however there is little effect on this compared to the electron attenuation as the mass of the ions is far greater. The actual insert current itself is $J_0\pi R^2 G(\Phi)$ (there is a small correction for those electrons that go through the plasma grid aperture) and the extracted electron current is $J\pi r^2$ where r is the aperture radius (which less than R). The ratio of extracted current, I_{ex}, to insert current, I_{in}, is:

$$\frac{I_{ex}}{I_{in}} = \frac{r^2}{R^2 G(\Phi)}\exp\left[-\frac{2e\,G(\Phi)\int_0^{d_i} B\,dz}{\pi Rm v_e}\right] \qquad (28)$$

This is a similar result to that in [17] when Φ is negative.

The extraction system of negative ions and electrons is shown in figure 1 but is not discussed here as it is described elsewhere [20]. The co-extracted electrons are collected on the second electrode of the accelerator, while the negative ions continue onwards to form the extracted beam. At the end of the beam line which is about 2m in length, there is a calorimeter to measure the beam current [21] which can then be compared to the current calculated by the model.

4. Results and Discussion

The output from the model has been compared with existing data from SNIF where possible. In order to model the source as accurately as possible, the total magnetic field present in the source had to be closely represented in the model, despite the fact that a large percentage of this is due to the accelerator magnets in front of the source in SNIF. Measurements were taken of the field within the SNIF source, and it was shown to rise steadily to ~35Gauss at 175mm along then source axis, then make a sharp rise up to ~100Gauss at the plasma grid.

The model calculates a detailed description of the source parameters along the length of the source for different values of source gas pressure and RF net forward power, i.e. plasma density, electron temperature, plasma potential, current densities and species fractions. There is currently no mechanism for measuring the actual amount of RF power coupled to the plasma and hence any system losses (not including plasma losses), therefore it has been assumed that all the forward power (i.e. that not reflected) is the same as the amount absorbed by the plasma i.e. P_{rf}. It should also be noted that it has been assumed that the negative ion temperature is equal to the electron temperature, since there is currently no measure of the negative ion temperature. Example outputs are shown in the following figures, using a source gas pressure of 0.6Pa, equivalent to a gas flow rate of $1.67 \times 10^{-7} m^3 s^{-1}$ on SNIF.
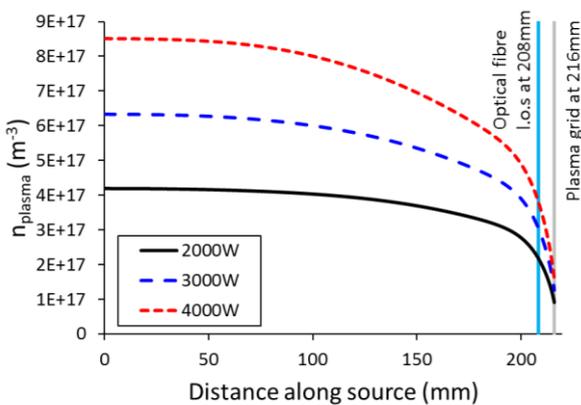
FIGURE 3. Model output of plasma density (= $n_{H-} + n_e$) along the source central axis at 0.6Pa source pressure and 2000W, 3000W and 4000W RF power
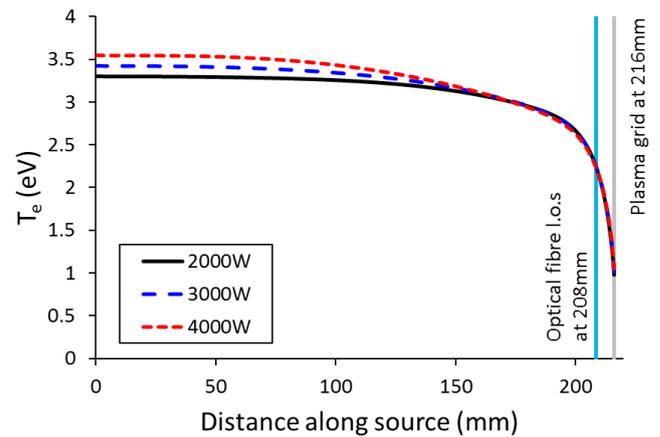
FIGURE 4. Model output of electron temperature along the source central axis at 0.6Pa source pressure and 2000W, 3000W and 4000W RF power. Note that T_e and T_{H-} are assumed equal whereas T_i (positive ion temperature) is assumed to be equal to the gas temperature and applies to the three species
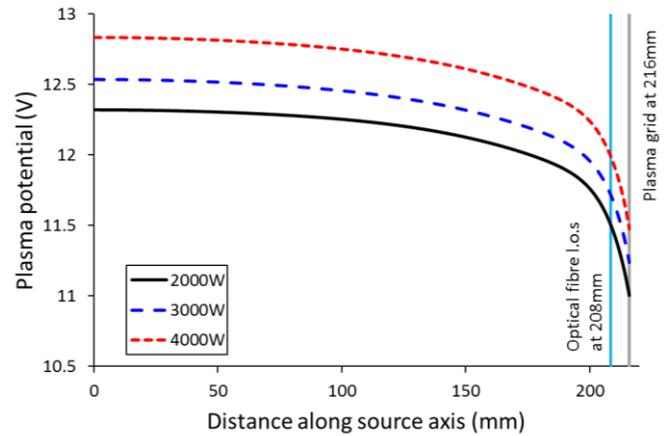
FIGURE 5. Model output of plasma potential along the source central axis at 0.6Pa source pressure and 2000W, 3000W and 4000W RF power
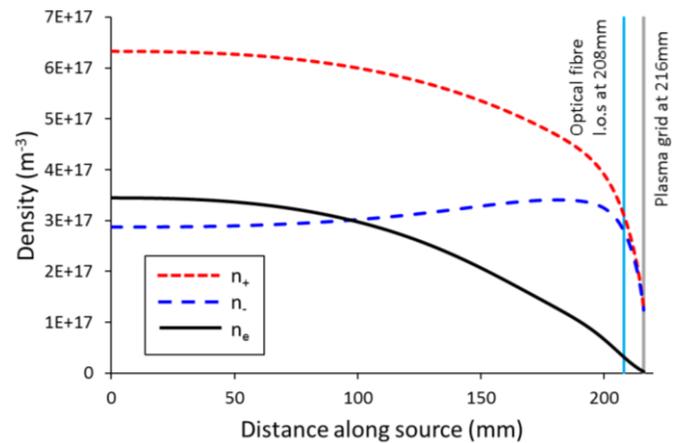
FIGURE 6. Model output of total positive ion density n_+, negative ion density n_- and electron density n_e along the source central axis at 0.6Pa source pressure and 3000W RF power
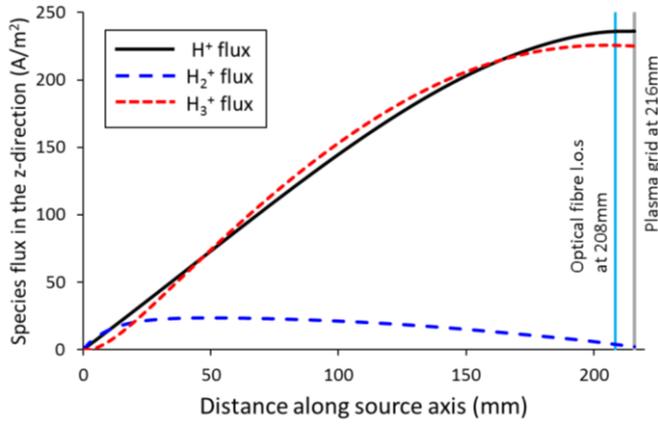
FIGURE 7. Model output of the positive species fluxes in the z-direction towards the plasma grid at 0.6Pa source pressure and 3000W RF power

From figures 3-5 it can be deduced that the large field magnitude near the grid causes a sharp drop in plasma density and electron temperature, and a small drop in plasma potential. For the case of plasma density and potential it is evident that a higher RF power increases the value at the antenna end as well as that at the grid, however for the electron temperature the RF power level only affects the temperature at the antenna. Figures 4 and 5 show that for plasma temperatures of ~3.5eV, the plasma potential is between 12-13V, as calculated by equation 7. Note that the plasma density is defined as the total positive particle density which is equal to the total negative particle density i.e. $n_{plasma} = n_{H^+} + n_{H_2^+} + n_{H_3^+} = n_{H^-} + n_e$. Figure 6 shows that the positive and negative ion and electron densities sharply drop close to the grid, again as a result of the high magnetic field, although there is a small rise in the negative ion current density before this sharp drop. Figure 7 shows that as the model steps through the source, there is a rise in H^+ and H_3^+ flux to the plasma grid, however it is evident that relatively few H_2^+ ions are produced in the z-direction (along the source axis). Note that because this model is 1D only, the species fluxes in the x and y directions (radial) are not known, therefore the fluxes in figure 7 are not the total flux magnitudes. Shown in all the above plots are the positions of the plasma grid and the diagnostic optical fibre line of sight relative to the source axis.

Currently it is not possible to experimentally measure the source parameters shown in figures 3-7 at different positions along the axis, therefore the model cannot yet be fully verified by experimental data. However it has been possible to measure a number of parameters using the diagnostic optical fibre and spectroscopy at the fixed position of 208mm close to the plasma grid as shown in figures 3-7. The existing SNIF data which has been modelled includes measurements of the negative ion current (beam current) from thermal analysis of the copper beam dump, and the extracted electron current (i.e. grid 2 current), at different source pressures and RF power settings, as well as the parameters measured by spectroscopy.

This data is the same as presented in reference [20]. The beam current and extracted electron current are also affected by the bias insert voltage, therefore data has also been taken varying this parameter.

The following figures show the comparison between the SNIF data and the corresponding model outputs where a comparison has been possible. It should be noted that figures 10 – 14 use data taken by spectroscopy, whereas plots 8, 9, 15 and 16 contain electrical and thermal data. The thermal data for beam current calculated by ANSYS (figures 8 and 15) has been corrected for stripping losses in the accelerator and vacuum tanks, and therefore represents the current after extraction.
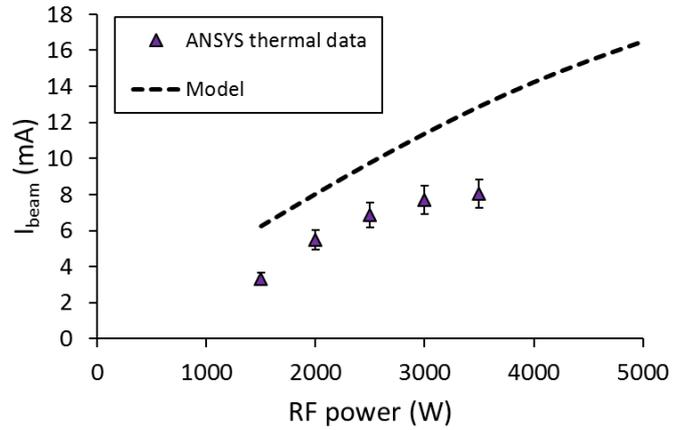
FIGURE 8. Results from the model compared with data from SNIF at 0.6Pa source pressure and varying RF power for extracted beam current (H⁻ ion current)
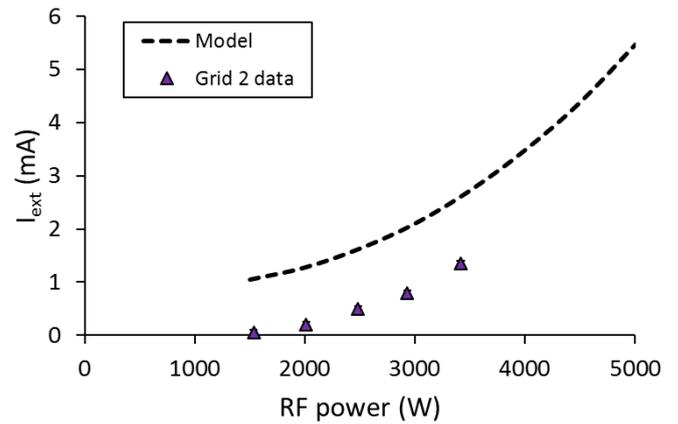
FIGURE 9. Results from the model compared with data from SNIF at 0.6Pa source pressure and varying RF power for extracted electron current. Note that there are error bars present on the plot but the only source of error here is the grid 2 power supply precision and therefore the error bars are too small to be clearly visible.
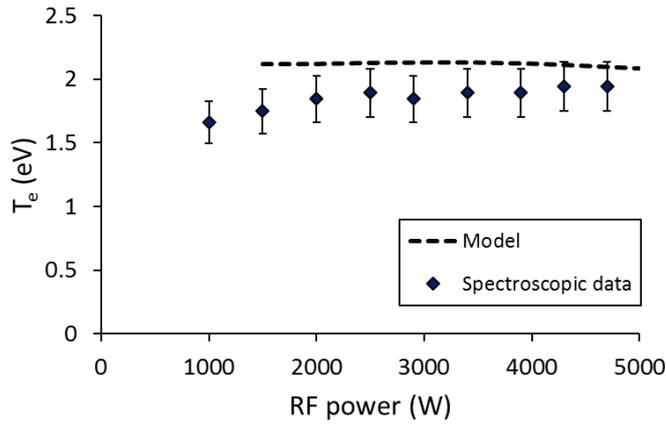
FIGURE 10. Results from the model compared with data from SNIF at 0.6Pa source pressure and varying RF power for electron temperature

FIGURE 11. Results from the model compared with data from SNIF at 0.6Pa source pressure and varying RF power for electron density

FIGURE 12. Results from the model compared with data from SNIF at 0.6Pa source pressure and varying RF power for the ratios of H^+ and H_3^+ densities to total positive particle density.
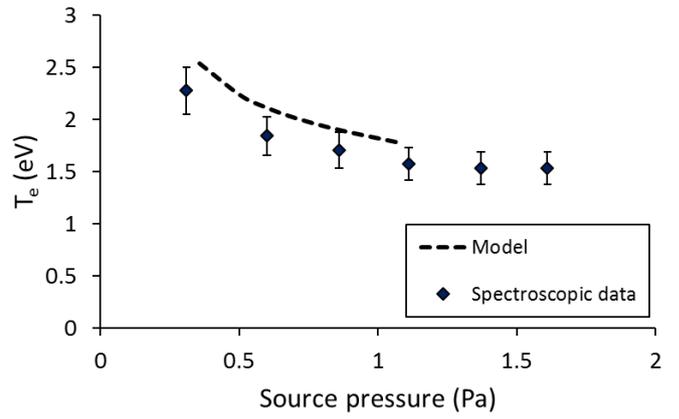
FIGURE 13. Results from the model compared with data from SNIF at 2000W RF power and varying source pressure for electron temperature
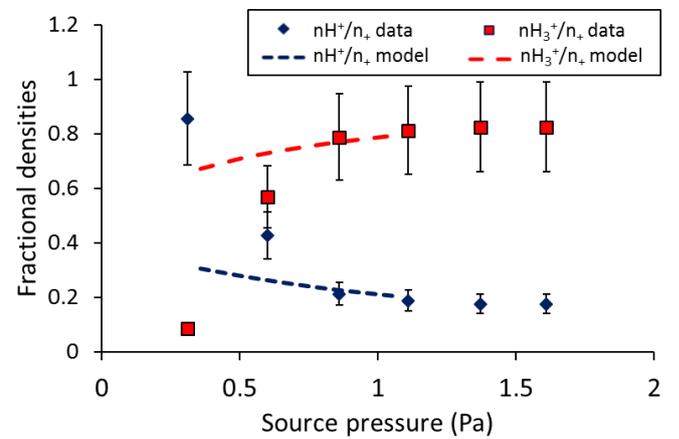
FIGURE 14. Results from the model compared with data from SNIF at 2000W RF power and varying source pressure for the ratios of H^+ and H_3^+ densities to total positive particle density.
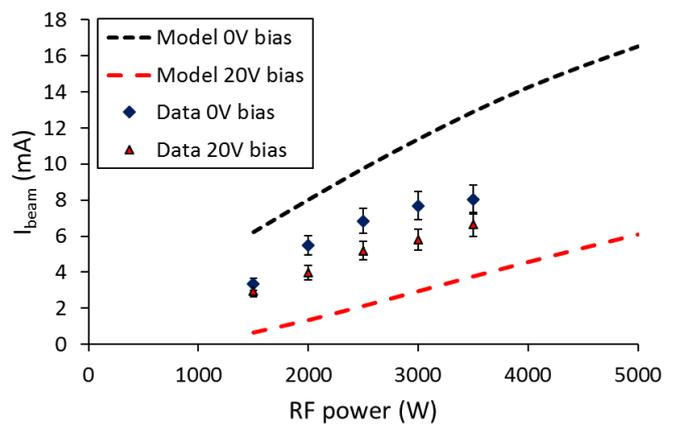
FIGURE 15. Model output compared with SNIF data showing the effects of the bias power supply on negative ion attenuation for a fixed source pressure of 0.6Pa and varying RF power
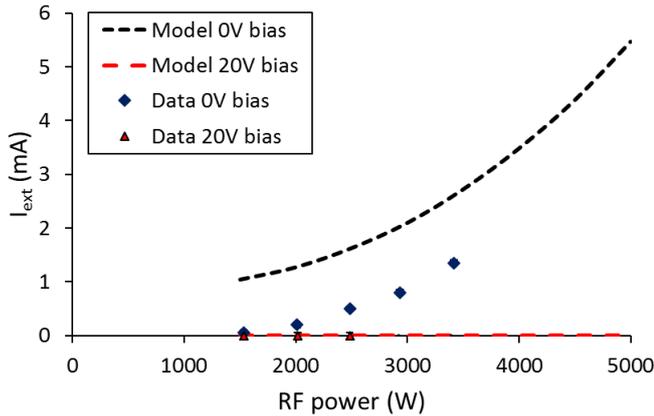
FIGURE 16. Model output compared with SNIF data showing the effects of the bias power supply on electron attenuation for a fixed source pressure of 0.6Pa and varying RF power. Note that there are error bars present on the plot but the only source of error here is the grid 2 power supply precision and therefore the error bars are too small to be clearly visible.

Figures 8-16 show that the model output and experimental data are broadly in agreement. There are a few discrepancies between the model and the data, particularly the negative ion to electron ratio (figure 11). It should be noted that when varying the source pressure, the model would not operate beyond a pressure of 1.1Pa, hence in figures 13 and 14 the model trends stop at this point. It is believed that at these higher pressures the model becomes unstable, since it is operating at low power discharges relative to an arc discharge source, therefore further development may be needed.

All data presented in figures 10 - 14 were obtained from spectroscopy using a Yacora analysis as detailed in [20]. The Yacora code uses a collisional radiative model. Originally a Coronal model was used instead, but there was some doubt about the validity of this method, due to the high plasma density predicted by the model in the region of the optical fibre used for spectroscopic measurement; the Coronal model is only valid for plasma densities $\leq 10^{17} m^{-3}$ [22, 23, 24]. The fibre has a diameter of 200μm and is placed behind a 4.91mm diameter lens with a focal length of 15.15mm. This system has a full acceptance angle of 0.0132rad, and this has been accounted for in the model by taking an average of the temperature over the field of view of the lens around the centre of the fibre. In light of the remaining discrepancies seen between the model and data, an accurate Langmuir probe measurement of the data obtained by spectroscopy will also be required to verify the data, and if there is still disagreement at this stage then the model may need revising.

It is evident from figure 11 that there is a large discrepancy between the Yacora results and source model for the negative ion to electron ratio. The model predicts much higher negative ion density than electron density close to the plasma grid, whereas Yacora is indicating the opposite. The model result however is consistent with the fact that experimentally the source produces very few co-extracted electrons compared to negative ions, as is shown in figures 8 and 9. There is also strong evidence from experimental observations for the existence of negative ions in the source and that SNIF must be extracting a high number of negative ions over electrons because of the following:

- The beam produced by SNIF can be seen and has been recorded by cameras – an electron beam at ~30keV energy would not be seen.
- Given that the beam travels ~2m to the calorimeter, if it was an electron beam it would have been deflected by the Earth's magnetic field before reaching this point.

There is little that can be done to the model to obtain different results in terms of the input data since the geometry of the source is fixed and there is a heavy dependence on cross-sections which are well established [13]. We do not believe that there are any significant weaknesses in the hypothesis as the model is almost identical to that used for DC sources [6,7], which has accurately described the PINI and other sources. Once appropriate data is obtained from the Faraday cup for negative ion current and hence the ratio of negative ions to electrons, we may be able to draw stronger conclusions and resolve this discrepancy.

There was also a discrepancy between the data and model for the extracted electron current and beam current with source pressure (not shown), suggesting that there are additional interactions occurring within the biased insert region that are not fully understood, or that the modelling approach for the insert region is not appropriate. However, measuring the electron current density at the plasma grid from the end of the transport model before entering the insert region, the model does show that the current density does in fact decrease with increasing source pressure as shown in figure 17 below, strongly suggesting that the problem lies in the insert region part of the model.
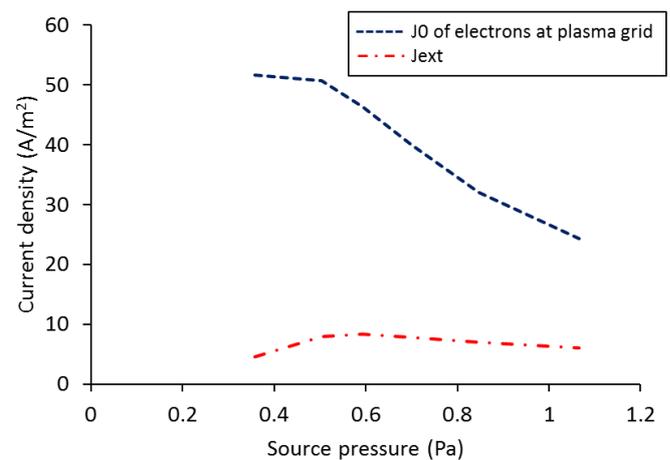
FIGURE 17. Model outputs of electron current density at the plasma grid and after extraction with source pressure (bias insert voltage = 0V)

In order to properly diagnose the issue and better understand the physics inside the insert region, more diagnostics will be needed e.g. a probe between the plasma grid and the insert. An improved modelling solution for the insert region may also be needed, despite the fact that the extracted electron current does follow the experimental data well when varying the RF power. Figures 15 and 16 also show that the model is correctly calculating electron and negative ion suppression with varying biased insert voltage, and that the electrons are suppressed by a much larger factor than the negative ions, as is reflected by the data.

5. Conclusion

A first attempt at modelling the SNIF ion source using one-dimensional fluid model has been presented here, and the output broadly agrees with the existing experimental data. Further data from SNIF will be required for verification of existing results, in particular measurements of the negative ion and electron density, as there is clearly a large discrepancy between the spectroscopic data and the model for these parameters. However the model does agree with the extraction data and thermal data, and the fact that we can see the beam with visible cameras is a strong indicator that negative ions are present. For an accurate measurement of the beam current and hence to verify the ratio of negative ions to electrons, a Faraday cup has been installed on the experiment in order to compare with the existing data obtained from thermal analysis. It is also desirable to take data with a Langmuir probe to verify the extraction data. There is currently no experimental plan to do this due to budget constraints and the fact that it may be challenging to install, however an alternative would be to use the biased insert itself as a probe. Further work is required in order to ensure that the model can run with source pressures above 1Pa without becoming unstable, and to better understand the discrepancy between extracted electron current with source pressure trend, which may also include additional data to be taken within the region between the plasma grid and the biased insert.

Acknowledgements

References

[1] Gudmundsson J T and Lieberman M A 1998 *Plasma Sources Sci. Technol.* **7** 83

[2] Bacal M, Bruneteau A M, Graham W G, Hamlton G W and Nachman M 1981 *J. Appl. Phys.* **52** *1247*

[3] Leung K N, Ehlers K W, Hauck C A, Kunkel W B and Lietze A L 1988 *Rev. Sci. Instrum.* **89** *453*

[4] Holmes A J T, Dammertz D and Green T S 1985 *Rev. Sci. Instrum.* **56** *1697*

[5] Holmes A J T, Green T S and Newman A F 1987 *Rev. Sci. Instrum.* **58** *1369*

[6] Surrey E and Holmes A J T 2015 *Plasma Sources Sci. Technol.* **24** 015035

[7] Surrey E and Holmes A J T 2015 *Plasma Sources Sci. Technol.* **24** 015036

[8] Epperlein E M and Haines M J 1986 *Phys. Fluids 29 1029*

[9] Turner I and Holmes A J T 2016, *AIP Conf. Proc.***1869** *020013*

[10] Leung K N, Hershowitz N and Mackenzie K R 1978 *Phys. Fluids* **18** *1045*

[11] Hjartarsen A T, Thorsteinsson E G, and Gudmundsson J T 2010 *Plasma Sources Sci. Technol.* **19** 065008

[12] Harbour P J 1978 *Culham Laboratory report CLM-P535, HMSO*

[13] IAEA AMDIS Aladdin database *https://www-amdis.iaea.org/ALADDIN*

[14] Hiskes J R and Karo A M 1990 *J. Appl.Phys.* **67** *6621*

[15] Karo A M and Hiskes J R 1986 *4th Int. Symp. on Production and Neutralisation of Negative Ions and Beams, Brookhaven (New York AIP)* 97

[16] Holmes A J T 1996 *Plasma Sources Sci. Technol.* **5** 453

[17] Haas F A and Holmes A J T 1991 *Plasma Phys. Control. Fusion* **33** 1197

[18] McAdams R et al, 2011, Plasma Sources Sci. Technol. **20**, 035023

[19] Tawara H, Itikawa Y, Mishimura H and Yoshino M 1990 *J Phys. Chem.* **19** *617*

[20] Zacks J, Fantz U, Farley T, Turner I, McAdams R and Wunderlich D 2016, *AIP Conf. Proc.***1869** *030047*

[21] Zacks J et al 2015, *AIP Conf. Proc. 1655, 030012*

[22] Fantz U 2006 Plasma Sources Sci. Technol. **15**, S137-147

[23] Boivin R F, Kline J L and Scime E E 2001 Phys. Plasmas 8, 5303-5314

[24] Komppula J and Tarvainen O 2015 Plasma Sources Sci. Technol. **24**, 045008